Journal of
Composites Science

MDPI

Article

Numerical Analysis on Static Performances of Graphene Platelet-Reinforced Ethylene-Tetrafluoroethylene (ETFE) Composite Membrane Under Wind Loading

Yu Wang [1], Jiajun Gu [2], Xin Zhang [2], Jian Fan [2], Wenbin Ji [2] and Chuang Feng [1,*]

[1] College of Civil Engineering, Nanjing Tech University, Nanjing 211816, China; wy153472511@outlook.com
[2] China Construction Third Engineering Bureau Group Co., Ltd. (Shenzhen), Shenzhen 518131, China; zjsjsz@cscec.com (J.G.); ycxuyiming@gmail.com (X.Z.); zhaoet@whu.edu.cn (J.F.); jiwenbin07@cscec.com (W.J.)
* Correspondence: chuang.feng@njtech.edu.cn

Abstract: This study examines the static performances of a graphene platelet (GPL)-reinforced ethylene tetrafluoroethylene (ETFE) composite membrane under wind loadings. The wind pressure distribution on a periodic tensile membrane unit was analyzed by using CFD simulations, which considered various wind velocities and directions. A one-way fluid–structure interaction (FSI) analysis incorporating geometric nonlinearity was performed in ANSYS to evaluate the static performances of the composite membrane. The novelty of this research lies in the integration of graphene platelets (GPLs) into ETFE membranes to enhance their static performance under wind loading and the combination of micromechanical modelling for obtaining material properties of the composites and finite element simulation for examining structural behaviors, which is not commonly explored in the existing literature. The elastic properties required for the structural analysis were determined using effective medium theory (EMT), while Poisson's ratio and mass density were evaluated using rule of mixtures. Parametric studies were carried out to explore the effects of a number of influencing factors, including pre-strain, attributes of wind, and GPL reinforcement. It is demonstrated that higher initial strain effectively reduced deformation under wind loads at the cost of increased stress level. The deformation and stress significantly increased with the increase in wind velocity. The deflection and stress level vary with the wind direction, and the maximum values were observed when the wind comes at 15° and 45°, respectively. Introducing GPLs with a larger surface area into membrane material has proven to be an effective way to control membrane deformation, though it also results in a higher stress level, indicating a trade-off between deformation management and stress management.

Keywords: graphene platelets; ETFE; fluid–structure interaction; wind pressure distribution

Citation: Wang, Y.; Gu, J.; Zhang, X.; Fan, J.; Ji, W.; Feng, C. Numerical Analysis on Static Performances of Graphene Platelet-Reinforced Ethylene-Tetrafluoroethylene (ETFE) Composite Membrane Under Wind Loading. *J. Compos. Sci.* **2024**, *8*, 478. https://doi.org/10.3390/jcs8110478

Academic Editor: Francesco Aymerich

Received: 14 September 2024
Revised: 12 November 2024
Accepted: 15 November 2024
Published: 18 November 2024

1. Introduction

Tensile membrane structures have gained significant attention in both architectural and engineering fields due to their lightweight nature, aesthetic appeal, and ability to cover large spans with minimal material usage [1,2]. These structures, typically composed of materials like ethylene tetrafluoroethylene (ETFE) and PVC-coated polyester, are widely utilized in applications ranging from sports arenas to exhibition pavilions [3,4]. The inherent flexibility of membrane structures allows for innovative designs, but this flexibility also presents challenges in terms of structural stability and response to environmental loads, particularly wind forces [5]. Research on the behavior of tensile membrane structures under various loading conditions has been extensively carried out. Numerical methods, particularly finite element analysis (FEA), have been pivotal in advancing the understanding of how these structures behave under wind [6], snow [7,8], and other environmental loads. Studies have been focused on optimizing membrane shape [9,10] and understanding the impact of pre-stress levels on the overall stability and durability of the structure.

Despite significant progress, one of the primary challenges that remains is to enhance the mechanical properties of the membrane materials themselves [11,12]. Researchers and industry professionals have explored various approaches to improve the performance of membrane materials, including the incorporation of advanced materials that can provide higher strength, better durability, and enhanced resistance to environmental aging. Among these advanced materials, carbon-based nanomaterials, such as carbon nanotubes (CNTs) and graphene (including its derivatives), have emerged as promising candidates due to their exceptional mechanical, thermal, and electrical properties [13–15]. Graphene, in particular, has attracted widespread attention due to its extraordinary strength and stiffness, coupled with its lightweight nature [16]. These characteristics make it an ideal reinforcement material for polymers and other composites. In recent years, extensive research has been conducted on the integration of graphene into various matrices, aiming to create composite materials with superior properties [17]. The effective enhancement of mechanical properties, such as tensile strength, Young's modulus, and fracture toughness, has been demonstrated in numerous studies where graphene has been incorporated into materials such as epoxy resins, polymers, and even metals [18,19].

The interest in graphene family composites has extended into the realm of structural applications [20–22], where the focus has been on developing materials that can withstand higher loads while maintaining or even reducing weight. This has led to a growing trend on using graphene family fillers as reinforcement in tensile membrane structures [23]. Graphene platelets (GPLs), which are small, flat pieces of graphene, offer several advantages over pure graphene when used as reinforcement in composites. Unlike single-layer graphene, GPLs are easier to disperse in polymer matrices, ensuring more uniform distribution and improving the overall mechanical properties of the composite. GPLs are also more cost-effective and easier to process compared to pure graphene, which often requires advanced fabrication techniques. These advantages make GPLs an ideal reinforcement for lightweight and flexible materials, such as membranes. The combination of GPLs with traditional membrane materials like ETFE offers the potential for significantly improved performance, particularly in terms of resistance to environmental loading and longevity of the structure. However, despite the promising potential of GPLs-enhanced membranes, there remains a gap in the research regarding to the specific application of these materials in tensile membrane structures subjected to wind actions. While several studies have investigated the mechanical properties of GPLs composites, limited research has focused on their performance under real-world conditions, such as wind loading. This gap in knowledge is critical, as the response of the membrane structure to wind loads can significantly affect its stability and performance over time.

This research addresses the identified gap by investigating the wind-induced static performances of a periodic GPL-reinforced ETFE composite membrane unit, as depicted in Figure 1a, surrounding the facades of a building, as shown in Figure 2. Detailed dimensions of the unit are provided in the multiview orthographic projection in Figure 1b. The composite membrane unit is composed of four individual pieces with a thickness of 400 μm, with all edges of each piece fixed to a steel support structure. To enhance the membrane's mechanical properties, GPLs are incorporated. The tensile modulus of the GPL reinforced ETFE composite is predicted using effective-medium theory (EMT), while rule of mixtures is employed to approximate the composite's Poisson's ratio and density. A one-way fluid–structure interaction analysis in ANSYS is conducted to perform a parametric study on the static behaviors of the composite membrane.

This study not only examines the wind pressure distribution on the membrane but also investigates how the introduction of GPLs affects the deformation of the structure. This research aims to provide a comprehensive understanding of how GPL-reinforced ETFE composite membranes perform under wind load. The findings from this study will contribute to ongoing efforts to enhance the performance of the composite membrane, offering new insights into the application of advanced materials like graphene in real-world architectural and engineering contexts.

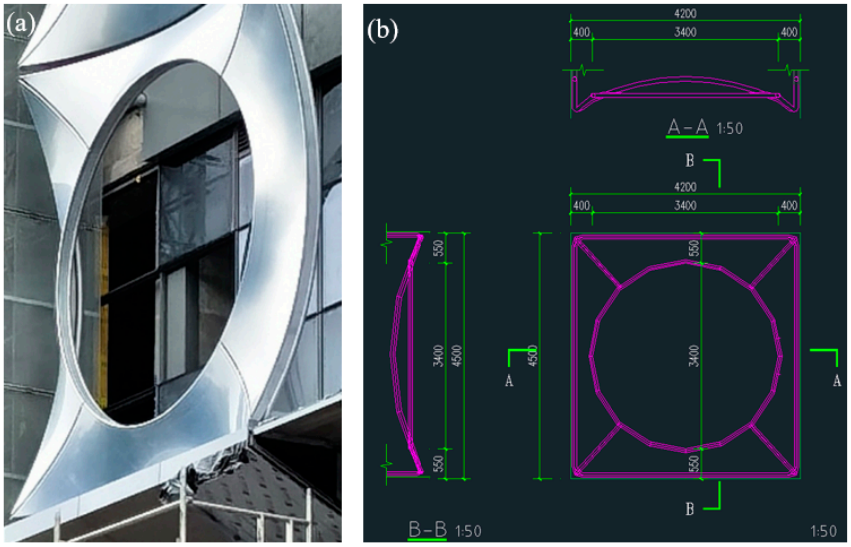

Figure 1. (**a**) GPL/ETFE composite membrane unit; (**b**) multiview orthographic projection.

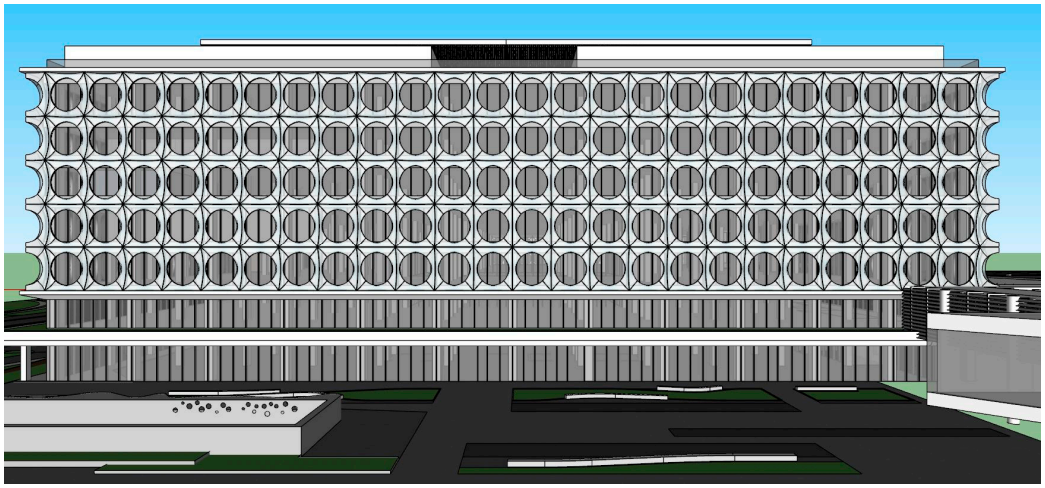

Figure 2. Building surrounded by periodic GPL/ETFE composite tensile membrane units.

2. Effective Mechanical Properties of GPL Reinforced ETFE Composites

Effective medium theory (EMT) has demonstrated its capability to accurately predict the mechanical properties of composites reinforced with GPLs [24]. According to EMT, the Young's modulus of these composites can be derived by solving the following scalar equations [25]:

$$\varnothing_m \frac{L_m - L_e}{L_m + (\frac{1}{3})(L_m - L_e)} + \frac{1}{3}\varnothing_f \sum_{k=1}^{3} \frac{L_k - L_e}{L_e + S_{kk}(L_k - L_e)} = 0 \quad (1)$$

In this equation, L_k $(k = 1, 2, 3)$ represents the components of the associated moduli tensor, while S_{kk} $(k = 1,\ 2,\ 3)$ refers to the components of Eshelby's tensor corresponding to the GPL reinforcement within the local coordinate system. The volume fraction is represented by ϕ, and the subscripts "m", "f", and "e" refer to the matrix, filler, and effective composite, respectively.

By substituting the relevant elastic parameters into Equation (1), the Young's modulus of the composites can be determined as:

$$\varnothing_m \frac{E_m - E_e}{E_e + (\frac{1}{3})(E_m - E_e)} + \frac{1}{3}\varnothing_f \sum_{k=1}^{3} \frac{E_k - E_e}{E_e + S_{kk}(E_k - E_e)} = 0 \quad (2)$$

where E_e stands for the effective Young's modulus of the composites. To account for the imperfect bonding between GPL fillers and the polymer matrix, the modulus for the coated GPL is adjusted as:

$$E_k^{(c)} = E_0^{(int)} \left[1 + \frac{(1 - \varnothing_{int}) \left(E_k - E_0^{(int)} \right)}{\varnothing_{int} S_{kk} \left(E_k - E_0^{(int)} \right) + E_0^{(int)}} \right] \quad k = 1, 2, 3 \tag{3}$$

The Young's modulus of the interphase is denoted by $E_0^{(\mathrm{int})}$. The coated GPLs' modulus $E_k^{(\mathrm{c})}$ should replace the pristine GPLs' Young's modulus E_k in Equation (2).

The rule of mixtures is employed to estimate the Poisson's ratio and mass density of the GPL-reinforced composites:

$$\begin{aligned} v_e &= \varnothing_m v_m + \varnothing_f v_f \\ \rho_e &= \varnothing_m \rho_m + \varnothing_f \rho_f \end{aligned} \tag{4}$$

In the current paper, unless specifically indicated, the following parameters will be adopted:

- The mechanical properties of the ETFE are E_{m} = 0.9 GPa, ν_{m} = 0.305, ρ_{m} = 1700 kg/m^3, respectively;
- The mechanical properties of the GPL are selected as $E_1 = E_2$ = 1.01 TPa, E_3 = 101 TPa, ν_{GPL} = 0.175, ρ_{GPL} = 2200 kg/m^3, respectively;
- The weight fraction of GPL f_{GPL} is 1.0%;
- The dimensions of GPL are selected as $t_{\mathrm{GPL}} = 5 \times 10^{-8}$ m, $D_{\mathrm{GPL}} = 8.1967 \times 10^{-6}$ m;
- The membrane is pre-stretched in both in-plane directions with 0.5% initial strain;
- The angle between wind direction and y axis is 0°.

3. Fluid–Structure Interaction Simulation of Membrane Unit

A comprehensive simulation setup was developed in this project, enabling a detailed examination of the static performances of the membrane when subjected to wind forces. The one-way fluid–structure interaction approach used in the analysis is computationally efficient, providing accurate results while minimizing the computational resources required. This method is particularly suitable for applications where the structural deformation does not significantly alter the fluid flow field, making it a practical choice for optimizing the design and performance of membrane structures under wind loads. In the following sections, the simulation setup, including geometry and model configuration, numerical wind tunnel simulation and structural analysis will be introduced.

The fluid–structure interaction (FSI) model set up in Ansys focused on a periodically repeating membrane, specifically designed to study wind-induced behaviors. The Design Modeler within Ansys is utilized to model a single unit of the membrane unit, rather than the entire building surface. This membrane unit repeats in two orthogonal directions, x and z, enabling the accurate simulation of the structure's periodic nature without the computational expense of a full-scale model. The overall configuration of the model is generally a parallelepiped, a shape chosen for its simplicity and compatibility with the periodic boundary conditions applied later in the simulation. The surrounding fluid domain is modeled to encapsulate the membrane unit, providing a comprehensive environment for analyzing the interaction between fluid flow and the membrane. The details of the geometry for the FSI model of the periodic tensile membrane structure unit are shown in Figure 3.

To simulate the wind forces acting on the membrane structure, Ansys Fluent is employed for a numerical wind tunnel simulation. The SST k-omega turbulence model is selected from the viscous model options, particularly well-suited for this scenario due to its robustness in capturing complex flow behaviors, such as boundary layer separation and reattachment. The fluid medium, representing air, flows around the membrane structure, simulating realistic wind conditions. The choice of the SST k-omega model ensures

the accurate resolution of the turbulent flows around the membrane, which is critical for understanding the impact of wind forces on the structure.

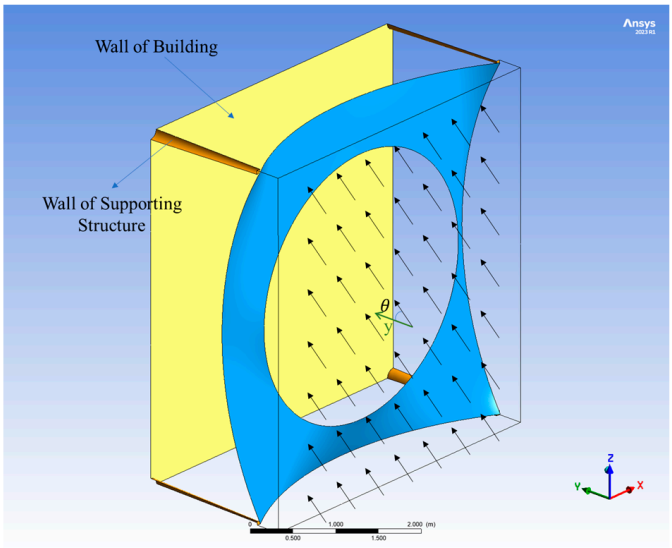

Figure 3. GPL/ETFE composite membrane with boundary conditions for numerical wind tunnel simulation.

A key aspect of the model setup involves the precise definition of boundary conditions. The details of these boundary conditions in the numerical wind tunnel simulation are shown in Figure 3. The model is designed with periodic boundary conditions on the left and right sides, as well as on the top and bottom, replicating the infinite repetition of the membrane structure. This setup allows for a more realistic and computationally efficient simulation. The front face of the model is defined as the inlet, where the wind enters the domain. The deviation of the wind direction from the y axis is denoted by θ. The inlet boundary conditions specify the turbulence intensity at 15% and the turbulent viscosity ratio at 10, which are typical values for simulations representing real-world wind tunnel conditions.

The rear face of the model includes the building surface and its supporting structures, both treated as walls with a no-slip condition, ensuring no relative motion between the fluid and these surfaces. The roughness of these walls is modeled using standard roughness models, with specific roughness heights and constants (1 m and 0.5, respectively) to replicate actual physical conditions. Similarly, both sides of the membrane are also treated as no-slip stationary walls, but with a reduced roughness height of 0.1 m to account for the different material properties and surface conditions of the membrane compared to the support structures.

The structural analysis portion of the model is conducted in Ansys Mechanical 2023 R1. The membrane material is defined with properties tailored to accurately reflect its physical behavior under wind loads, and the mesh is generated with sufficient resolution to capture the membrane's deformation precisely. Boundary conditions for the structural analysis include fixed supports at the edges and connections, ensuring that the membrane remains securely anchored during the simulation, as shown in Figure 4. ANSYS Parametric Design Language (APDL) is employed to apply a pre-strain to the membrane, simulating the initial tension that would be present in a real-world scenario. This pre-strain is critical to the membrane's structural integrity, influencing how it deforms under load.

A one-way fluid–structure interaction (FSI) approach is utilized to analyze the deformation of the tensile membrane structure unit subject to wind load. This method involves running the numerical wind tunnel simulation as described in the previous section to achieve the steady-state status of the fluid domain. The pressures exerted on the membrane surfaces by the fluid flow are then transferred as load inputs into the structural analysis. The static pressure data obtained from the fluid analysis is used as a load in the structural analysis, allowing for accurate prediction of the membrane's response to wind forces. Geometric nonlinearity is enabled in the structural analysis to account for the large deformations often experienced by membrane structures, ensuring that the simulation results are both realistic and reliable.

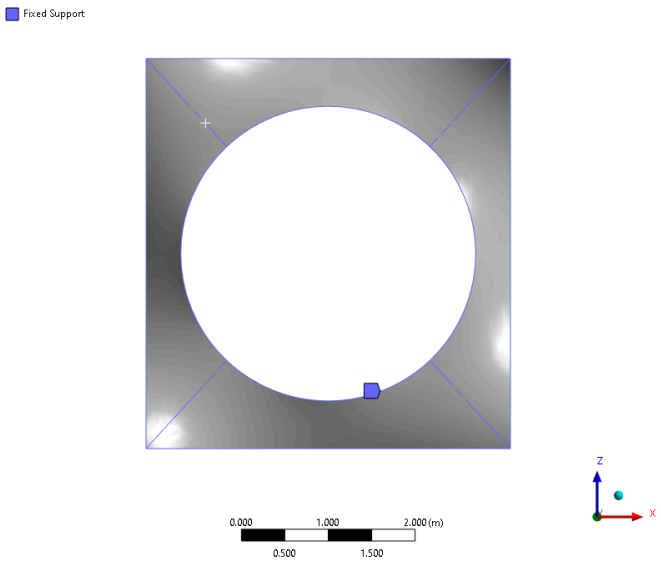

Figure 4. Boundary conditions of the structural analysis.

4. Results and Discussion

4.1. Effect of Pre-Stretching

The influence of initial strain on the deformation and stress distribution of the membrane was thoroughly examined. Various FSI cases with different initial strain levels, ranging from 0.1% to 1.0%, were simulated. The maximum deflection, maximum von Mises stress, and average von Mises stress on the membrane surface were extracted and plotted against the initial strain, as shown in Figure 5. The black line with squares represents the maximum deflection, which decreases significantly as the initial strain increases from 0.1% to 1.0%, showing a 79.19% reduction. This indicates that higher initial strain reduces structural deformation under wind loads. Conversely, the blue lines with rounds and hexagons illustrate that both the maximum and average von Mises stresses rise with increasing initial strain. The deformation and distribution of von Mises stress on ETFE tensile membrane with 0.1% and 1.0% initial strain subjected to 10 m/s wind load is presented in Figures 6 and 7. The finding underscores the critical balance that must be struck by designers: while higher initial strain can mitigate deformation, it also increases stress within the membrane. Therefore, selecting the optimal initial strain level is crucial to minimizing deformation while preventing excessive stress that could lead to structural failure under wind loads.

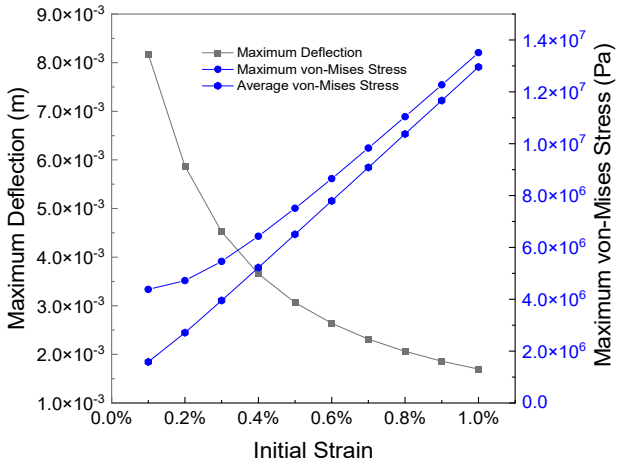

Figure 5. Effects of pre-stretching on maximum deflection and von Mises stress of membrane surface.

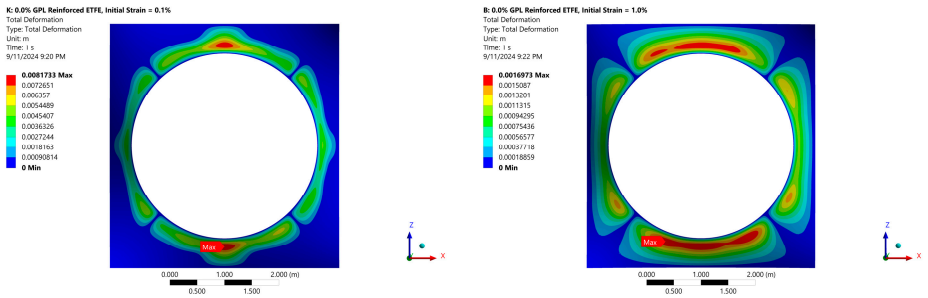

Figure 6. Deformation of ETFE composite membrane unit with different initial strains under 10 m/s wind: (**a**) initial strain = 0.1%; (**b**) initial strain = 1.0%.

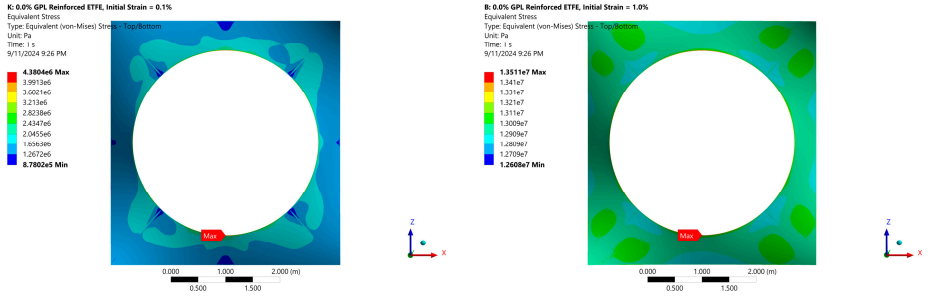

Figure 7. Distribution of von Mises stress of ETFE composite membrane with different initial strains under 10 m/s wind: (**a**) initial strain = 0.1%; (**b**) initial strain = 1.0%.

4.2. Effects of Wind Loading Conditions

In this section, the effect of wind conditions, including velocity and direction, on the maximum deformation and maximum von Mises stress of the membrane structure will be analyzed. To analyze the effect of wind velocity on the static behavior of the ETFE membrane structure unit, a set of FSI cases, in which the wind blows perpendicularly to the membrane at different speeds, ranging from 10 m/s to 30 m/s, were simulated. As the wind speed increases, the membrane's maximum deformation grows from 0.00307 m to 0.01933 m, while the maximum von Mises stress rises from 7.5077 MPa to 15.092 MPa, as shown in Figure 8a. The primary reason for this increase in deformation and stress lies in the corresponding rise in static pressure on both the windward and leeward sides of the membrane. As shown in Figure 8b, as the wind speed escalates from 10 m/s to 30 m/s, the average static pressure on the windward side increases significantly from 10.14316 Pa to

94.27328 Pa. Simultaneously, the average static pressure on the leeward side drops from −149.67 Pa to −1358.2178 Pa.

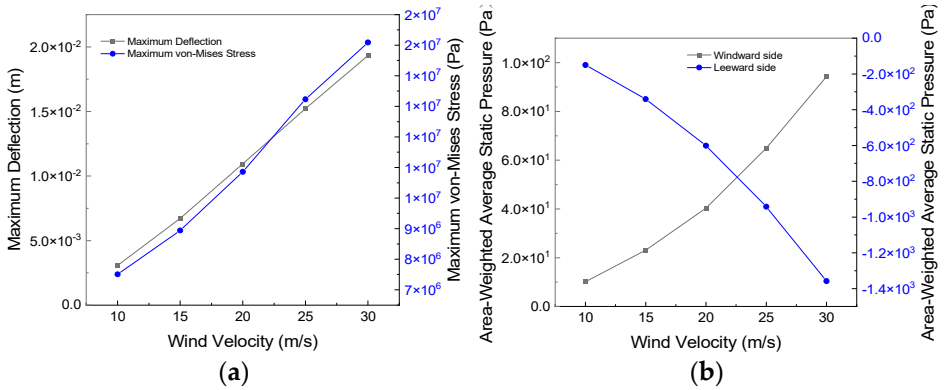

Figure 8. Effect of wind velocity on: (**a**) maximum deflection and von Mises stress; (**b**) area-weighted average static pressure on windward size and leeward side of ETFE composite membrane.

Next, the impact of wind direction on the membrane's maximum deformation and maximum von Mises stress was examined by varying the angle θ between the wind direction and the y axis. The variation of maximum deflection and von Mises Stress on the ETFE tensile membrane unit with the wind direction is given in Table 1. As the angle between wind direction and y–axis increases from 0° to 15°, the maximum deflection increases from 0.00638 m to 0.00838 m, representing a 31.35% increase. During the same interval, the maximum von Mises stress also rises from 8.9597 MPa to 9.5114 MPa, a 6.16% increase. This indicates that even a slight deviation in wind direction can significantly impact the membrane's response, likely due to an uneven distribution of pressure on the membrane surface. As the angle continues increasing from 15° to 90°, the maximum deflection on the membrane decreases steadily, reaching a minimum of 0.00138 m at 90°, which is an 83.53% decrease from the peak deflection at 15°. The maximum von Mises stress shows less fluctuation as the angle increases from 15° to 45°, with some minor variations, but overall does not change substantially. However, beyond 45°, the stress gradually decreases, reaching 6.841 MPa at 90°, representing a 28.74% reduction from the maximum observed at 45°.

Table 1. Maximum deflection and von Mises stress of ETFE composite membrane subjected to 15 m/s wind in different directions.

Wind Direction θ (°)	Maximum Deflection (m)	Maximum von Mises Stress (Pa)
0	0.00638	8,959,700
15	0.00838	9,511,400
30	0.00818	9,428,400
45	0.00737	9,600,000
60	0.00596	8,105,200
75	0.00325	7,351,200
90	0.00138	6,841,000

The change in deformation and stress is closely related to the area-weighted average static pressure on both the windward and leeward sides of the membrane. The variation of area-weighted average static pressure on both windward side and leeward side of the membrane with the increasing wind direction is tabulated in Table 2. The leeward side's average static pressure increases steadily from −338.99637 Pa at 0° to a mere −6.31158 Pa at 90°, corresponding to a significant reduction in the force exerted on the membrane. The windward side shows a more complex behavior. Initially, the static pressure increases as the angle increases, reaching a minimum of 90.20836 Pa at 60°. Beyond 60°, the pressure starts to decrease again, although not returning to its initial values. The detailed distribution of

static pressure on both windward and leeward sides of the membrane under wind load with different directions are presented in Figure 9.

Table 2. Area-weighted average static pressure on windward side and leeward side of ETFE composite membrane subjected to 15 m/s wind with different directions.

Wind Direction θ (°)	Area-Weighted Average Static Pressure (Pa)	
	Windward Side	Leeward Side
0	24.30616	−338.99637
15	42.65541	−341.09953
30	58.28871	−309.11767
45	48.41315	−304.77645
60	90.20836	−176.49991
75	18.08621	−93.92579
90	18.17405	−6.31158

The reduction in maximum deflection and von Mises stress as the wind direction angle increases beyond 15° can be attributed to the decreasing difference between the static pressure on the windward side and leeward side of the membrane, leading to a less significant load on the membrane. The complex behavior on the windward side contributes to the fluctuations in stress, particularly between 15° and 45°. Overall, this analysis underscores the importance of considering wind direction in the design and analysis of tensile membrane structures, as it can significantly affect both deformation and stress distribution.

4.3. Effects of GPL Reinforcements

After analyzing the effects of initial strain, and wind speed and direction, on the performance of tensile membrane structure unit, attention was directed towards enhancing the mechanical properties of ETFE by incorporating graphene platelets. The effect of the GPLs weight fraction in the GPL-reinforced ETFE on the performance of the tensile membrane structure unit was first investigated. The variation of the maximum deflection, von Mises stress, and von Mises strain of the GPL-reinforced ETFE tensile membrane structure unit subjected to 35 m/s wind coming from the y direction with the increasing GPL weight fraction is presented in Figure 10. As the weight fraction of GPLs in ETFE increases, the maximum deflection of the membrane decreases, as shown in Figure 10a. When the GPLs' weight fraction increases from 0% to 1%, the maximum deflection reduces from 0.002376 m to 0.001415 m. Concurrently, the maximum von Mises strain decreases from 0.02091 to 0.01405, while the maximum von Mises stress increases from 18.822 MPa to 28.015 MPa, as illustrated in Figure 10b. The primary reason for this is the enhancement of the material's stiffness due to the GPL reinforcement, where the Young's modulus of GPL-reinforced ETFE increases from 0.9 GPa to 1.99415 GPa as the GPL weight fraction rises from 0% to 1%, as shown in Figure 10a.

These findings highlight the effectiveness of GPLs in significantly improving the static performance of ETFE membranes, offering a potential pathway for optimizing membrane structures subjected to various environmental loads.

Next the effect of the aspect ratio of GPL reinforcement on the static performance of GPL-enhanced ETFE tensile membrane structure unit is analyzed. The thickness of the GPLs is fixed as 5×10^{-8} m, while the diameter-to-thickness ratio was varied from 100 to 1000. Figure 11 presents the impact of the GPL aspect ratio on the maximum deflection, Young's modulus, and von Mises strain of the membrane. As the GPLs' diameter-to-thickness ratio increases from 100 to 1000, the maximum deflection of the membrane decreases from 0.01677 m to 0.00867 m. Concurrently, the maximum von Mises strain reduces from 0.01575 to 0.01091, while the maximum von Mises stress rises significantly from 24.689 MPa to 40.391 MPa. These changes are primarily attributed to the enhancement in stiffness: when the diameter-to-thickness ratio of the GPLs increases from 100 to 1000, the Young's modulus

of the GPL-reinforced ETFE increases from 1.56735 GPa to 3.70168 GPa. This suggests that utilizing GPLs with a higher surface area to enhance ETFE is more effective in improving both the structural rigidity and the stress-bearing capacity of the membrane.

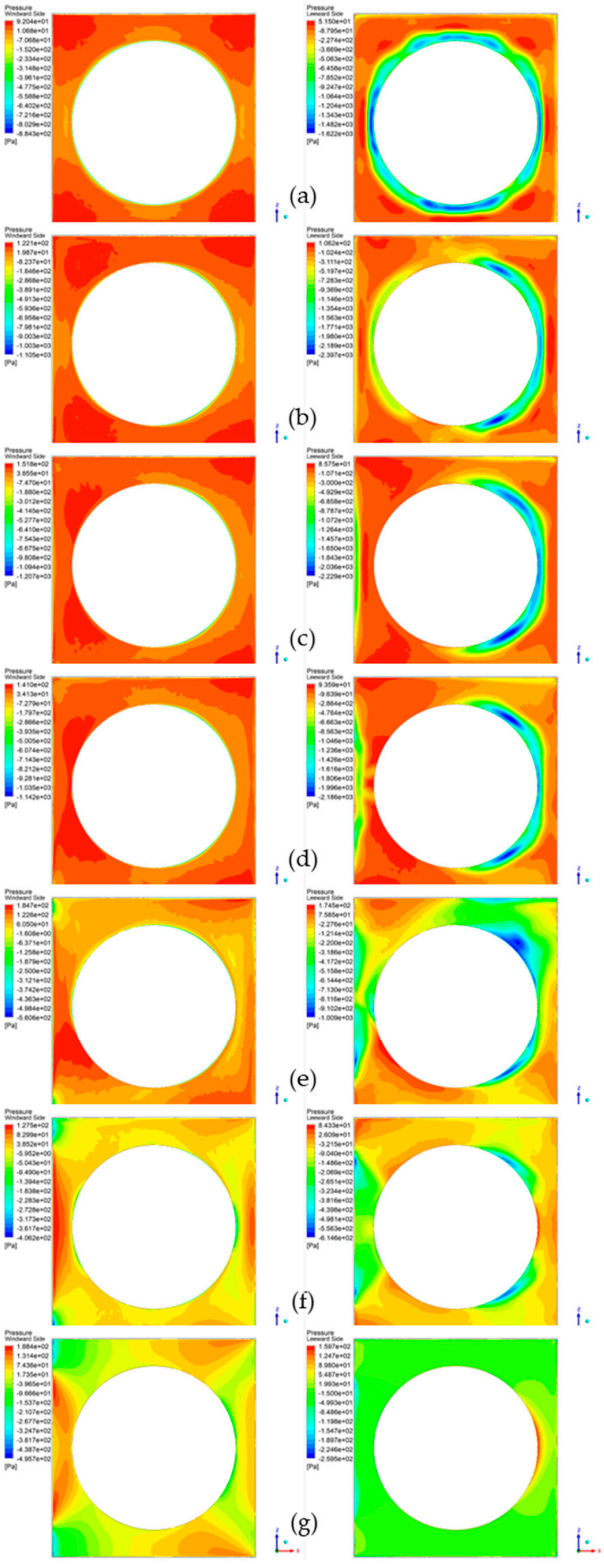

Figure 9. Static pressure distribution on the windward and leeward sides of ETFE tensile membrane subjected to 15 m/s wind with different directions: (**a**) $\theta = 0^\circ$; (**b**) $\theta = 15^\circ$; (**c**) $\theta = 30^\circ$; (**d**) $\theta = 45^\circ$; (**e**) $\theta = 60^\circ$; (**f**) $\theta = 75^\circ$; (**g**) $\theta = 90^\circ$.

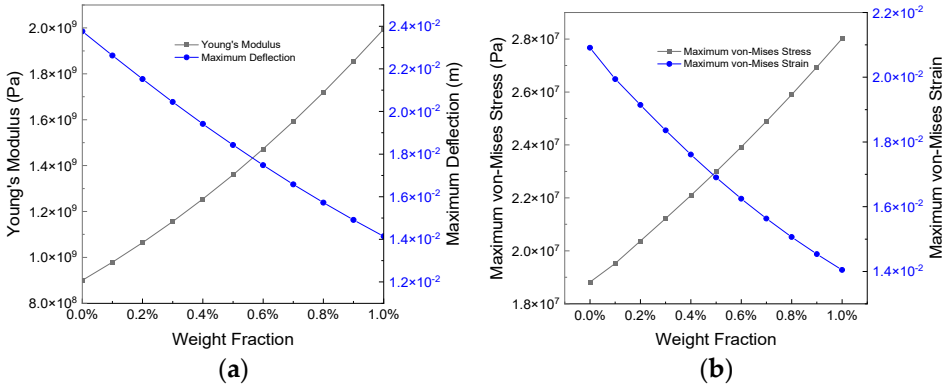

Figure 10. Effects of GPL concentration on (**a**) Young's modulus and the maximum deflection; (**b**) von Mises stress, and von Mises strain on GPL/ETFE composite membrane.

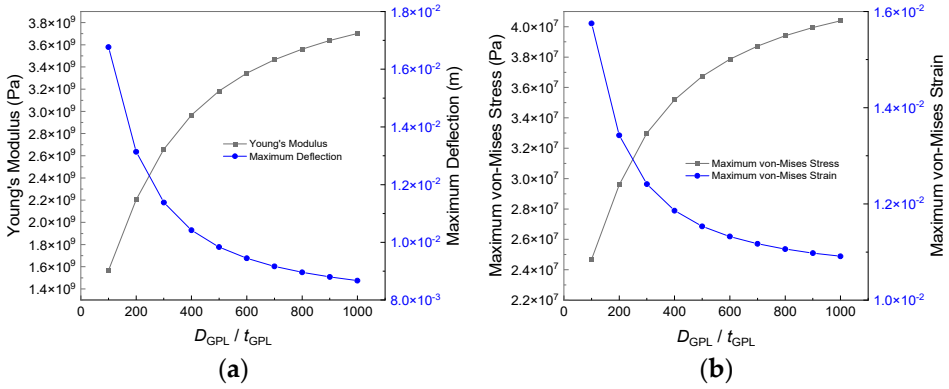

Figure 11. Effect of GPL aspect ratio on (**a**) Young's modulus and the maximum deflection; (**b**) Young's modulus, and von Mises strain of GPL/ETFE composite membrane subjected to 35 m/s wind.

5. Conclusions

This study explored the static performances of GPL-reinforced ETFE tensile membrane structures under various wind conditions. The findings demonstrated the significant influence of initial strain, wind speed, direction, and GPL reinforcements on the structural performance of the membrane. The results revealed that an increase in initial strain from 0.1% to 1.0% resulted in a 79.19% reduction in the maximum deflection under 10 m/s wind loads, though at the cost of increased stress levels. Wind conditions also play a crucial role in determining the membrane's response, with maximum deformation growing from 0.00307 m to 0.01933 m, and maximum von Mises stress intensifying from 7.5077 MPa to 15.092 MPa as wind speed increased from 10 m/s to 30 m/s. The orientation of the wind further influences the membrane's performance, with maximum deformation and stress occurring in specific directions.

The introduction of GPLs into the ETFE matrix significantly improved the mechanical properties of the membrane. By increasing the GPL weight fraction and aspect ratio, the membrane's stiffness is enhanced, leading to a substantial reduction in deformation and strain under wind loads. When the addition of GPLs increased from 0% to 1% by weight, the maximum deflection dropped from 0.002376 m to 0.001415 m. The increase of the GPLs' diameter-to-thickness ratio from 100 to 1000 resulted in the decreases from 0.01677 m to 0.00867 m in the maximum deflection. However, this also resulted in higher stress levels, indicating a trade-off between stiffness and stress management.

Overall, the incorporation of GPLs into ETFE membranes presents a promising approach for enhancing the structural performance of tensile membrane structures subjected to wind actions. These findings provide valuable insights for the design and optimization of membrane structures in architectural and engineering applications.

Author Contributions: Methodology, Y.W.; formal analysis, Y.W.; investigation, Y.W. and W.J.; resources, J.G., X.Z. and J.F.; data curation, J.G., X.Z., J.F. and W.J.; writing—original draft, Y.W.; writing—review and editing, J.G. and C.F.; supervision, C.F.; project administration, J.G. and C.F.; funding acquisition, C.F. All authors have read and agreed to the published version of the manuscript.

Funding: This research was funded by Department of Education, Jiangsu Province, China, and the China Construction Third Engineering Bureau Group (Shenzhen) Co., Ltd.

Data Availability Statement: The original contributions presented in the study are included in the article, further inquiries can be directed to the corresponding author.

Acknowledgments: The authors greatly acknowledge the financial support from the China Construction Third Engineering Bureau Group Co., Ltd. (Shenzhen) and the Innovative and Entrepreneurial Talents of Jiangsu Province of China.

Conflicts of Interest: Author Jiajun Gu, Xin Zhang, Jian Fan and Wenbin Ji was employed by the company China Construction Third Engineering Bureau Group Co., Ltd. (Shenzhen). The remaining authors declare that the research was conducted in the absence of any commercial or financial relationships that could be construed as a potential conflict of interest.

References

1. Xu, J.; Zhang, Y.; Yu, Q.; Zhang, L. Analysis and design of fabric membrane structures: A systematic review on material and structural performance. *Thin-Walled Struct.* **2022**, *170*, 108619. [CrossRef]
2. Lewis, W.J. Lightweight Tension Membranes—An Overview. *Proc. Inst. Civ. Eng.-Civ. Eng.* **1998**, *126*, 171–181. [CrossRef]
3. Lamnatou, C.; Moreno, A.; Chemisana, D.; Reitsma, F.; Clariá, F. Ethylene tetrafluoroethylene (ETFE) material: Critical issues and applications with emphasis on buildings. *Renew. Sustain. Energy Rev.* **2018**, *82*, 2186–2201. [CrossRef]
4. Taha, M.S.; Mamhusseini, A.A.; Abdullah, S. Exploring Tension Fabric Structure and Material—A Review of The Bigo Arena and Denver International Airport. *Eurasian J. Sci. Eng.* **2024**, *10*. [CrossRef]
5. Dutta, S.; Ghosh, S. Analysis and Design of Tensile Membrane Structures: Challenges and Recommendations. *Pract. Period. Struct. Des. Constr.* **2019**, *24*, 04019009. [CrossRef]
6. Hincz, K.; Gamboa-Marrufo, M. Deformed Shape Wind Analysis of Tensile Membrane Structures. *J. Struct. Eng.* **2016**, *142*, 04015153. [CrossRef]
7. Milošević, V.S.; Marković, B.L.; Bedon, C. Comparison of Point and Snow Load Deflections in Design and Analysis of Tensile Membrane Structures. *Adv. Civ. Eng.* **2020**, *2020*, 8810085. [CrossRef]
8. Sun, X.; He, R.; Wu, Y. Numerical simulation of snowdrift on a membrane roof and the mechanical performance under snow loads. *Cold Reg. Sci. Technol.* **2018**, *150*, 15–24. [CrossRef]
9. Dutta, S.; Ghosh, S.; Inamdar, M.M. Optimisation of tensile membrane structures under uncertain wind loads using PCE and kriging based metamodels. *Struct. Multidiscip. Optim.* **2017**, *57*, 1149–1161. [CrossRef]
10. Marbaniang, A.L.; Dutta, S.; Ghosh, S. Updated weight method: An optimisation-based form-finding method of tensile membrane structures. *Struct. Multidiscip. Optim.* **2022**, *65*, 169. [CrossRef]
11. Yuan, Y.; Zhang, Q.; Luo, X.; Gu, R. Experimental study on the mechanical properties of the reinforced transparent building membrane material STFE. *Constr. Build. Mater.* **2023**, *409*, 133849. [CrossRef]
12. Han, Y.; Xu, Y.; Zhang, S.; Li, T.; Ramakrishna, S.; Liu, Y. Progress of Improving Mechanical Strength of Electrospun Nanofibrous Membranes. *Macromol. Mater. Eng.* **2020**, *305*, 2000230. [CrossRef]
13. Gu, Z.; Wang, K.; Wei, J.; Li, C.; Jia, Y.; Wang, Z.; Luo, J.; Wu, D. Tensile properties of ultrathin double-walled carbon nanotube membranes. *Carbon* **2006**, *44*, 3315–3319. [CrossRef]
14. Rui, Y.; Guo, J.; Harwell, J.; Nakanishi, T.; Kotera, S.; Grady, B.P. Electrical, mechanical, and crystallization properties of ethylene-tetrafluoroethylene copolymer/multiwalled carbon nanotube composites. *J. Appl. Polym. Sci.* **2014**, *131*. [CrossRef]
15. Hasan, M.; Lee, M. Enhancement of the thermo-mechanical properties and efficacy of mixing technique in the preparation of graphene/PVC nanocomposites compared to carbon nanotubes/PVC. *Prog. Nat. Sci. Mater. Int.* **2014**, *24*, 579–587. [CrossRef]
16. Huang, X.; Yin, Z.; Wu, S.; Qi, X.; He, Q.; Zhang, Q.; Yan, Q.; Boey, F.; Zhang, H. Graphene-based materials: Synthesis, characterization, properties, and applications. *Small* **2011**, *7*, 1876–1902. [CrossRef]
17. Stankovich, S.; Dikin, D.A.; Dommett, G.H.; Kohlhaas, K.M.; Zimney, E.J.; Stach, E.A.; Piner, R.D.; Nguyen, S.T.; Ruoff, R.S. Graphene-based composite materials. *Nature* **2006**, *442*, 282–286. [CrossRef]
18. Papageorgiou, D.G.; Kinloch, I.A.; Young, R.J. Mechanical properties of graphene and graphene-based nanocomposites. *Prog. Mater. Sci.* **2017**, *90*, 75–127. [CrossRef]
19. Wang, H.; Xie, G.; Fang, M.; Ying, Z.; Tong, Y.; Zeng, Y. Electrical and mechanical properties of antistatic PVC films containing multi-layer graphene. *Compos. Part B Eng.* **2015**, *79*, 444–450. [CrossRef]
20. Wang, Y.; Feng, C.; Wang, X.; Zhao, Z.; Romero, C.S.; Dong, Y.; Yang, J. Nonlinear static and dynamic responses of graphene platelets reinforced composite beam with dielectric permittivity. *Appl. Math. Model.* **2019**, *71*, 298–315. [CrossRef]

21. Zhao, Z.; Feng, C.; Wang, Y.; Yang, J. Bending and Vibration Analysis of Functionally Graded Trapezoidal Nanocomposite Plates Reinforced with Graphene Nanoplatelets (GPLs). *Compos. Struct.* **2017**, *180*, 799–808. [CrossRef]
22. Wang, Y.; Feng, C.; Yang, J.; Zhou, D.; Liu, W. Static response of functionally graded graphene platelet–reinforced composite plate with dielectric property. *J. Intell. Mater. Syst. Struct.* **2020**, *31*, 2211–2228. [CrossRef]
23. Liu, Y.; Chen, X. Mechanical properties of nanoporous graphene membrane. *J. Appl. Phys.* **2014**, *115*, 034303. [CrossRef]
24. Hashemi, R.; Weng, G.J. A theoretical treatment of graphene nanocomposites with percolation threshold, tunneling-assisted conductivity and microcapacitor effect in AC and DC electrical settings. *Carbon* **2016**, *96*, 474–490. [CrossRef]
25. Xia, X.; Wang, Y.; Zhong, Z.; Weng, G.J. A frequency-dependent theory of electrical conductivity and dielectric permittivity for graphene-polymer nanocomposites. *Carbon* **2017**, *111*, 221–230. [CrossRef]